Identification of the dynamics of time-varying phase aberrations from time histories of the point-spread function

Doelman, Reinier; Klingspor, Måns; Hansson, Anders; Löfberg, Johan; Verhaegen, Michel

DOI
10.1364/JOSAA.36.000809

Publication date
2019

Document Version
Final published version

Published in
Journal of the Optical Society of America A: Optics and Image Science, and Vision

Research Article Vol. 36, No. 5 / May 2019 / Journal of the Optical Society of America A 809

Journal of the Optical Society of America A
OPTICS, IMAGE SCIENCE, AND VISION

Identification of the dynamics of time-varying phase aberrations from time histories of the point-spread function

Reinier Doelman,[1,*] Måns Klingspor,[2,3] Anders Hansson,[2] Johan Löfberg,[2] and Michel Verhaegen[1]

[1]Delft Center for Systems and Control, Delft University of Technology, Delft, The Netherlands
[2]Department of Electrical Engineering, Automatic Control, Linköping University, Linköping, Sweden
[3]e-mail: mans.klingspor@liu.se
*Corresponding author: r.doelman@tudelft.nl

Received 15 January 2019; revised 22 March 2019; accepted 22 March 2019; posted 25 March 2019 (Doc. ID 357867); published 18 April 2019

To optimally compensate for time-varying phase aberrations with adaptive optics, a model of the dynamics of the aberrations is required to predict the phase aberration at the next time step. We model the time-varying behavior of a phase aberration, expressed in Zernike modes, by assuming that the temporal dynamics of the Zernike coefficients can be described by a vector-valued autoregressive (VAR) model. We propose an iterative method based on a convex heuristic for a rank-constrained optimization problem, to jointly estimate the parameters of the VAR model and the Zernike coefficients from a time series of measurements of the point-spread function (PSF) of the optical system. By assuming the phase aberration is small, the relation between aberration and PSF measurements can be approximated by a quadratic function. As such, our method is a blind identification method for linear dynamics in a stochastic Wiener system with a quadratic nonlinearity at the output and a phase retrieval method that uses a time-evolution-model constraint and a single image at every time step.

https://doi.org/10.1364/JOSAA.36.000809

1. INTRODUCTION

Phase aberrations in optical systems cause blurring in the images taken with these systems. In order to improve the degraded image quality of an optical system due to aberrations, adaptive optics (AO) can be used to compensate for the aberrations online, or post-processing techniques can be used. For example, in (most) high-performance telescopes, these aberrations are wavefront (phase) aberrations induced by turbulence, misalignment, etc. To compensate for a phase aberration, by both online computations as well as post-processing of image data, information on this aberration is required. A classical method to obtain a phase aberration is using a Shack–Hartmann (SH) wavefront sensor [1] (see Fig. 1). This sensor measures the spatial derivatives of the wavefront, and from these measurements, the wavefront aberration itself can be estimated, as for example used in [2,3] for (quasi-)static phase aberrations. To optimally compensate for a dynamic aberration, a prediction of future aberrations has to be made. To predict the phase aberration at a future time step, a model that describes the (time) dynamics of the aberration is required. This model can be obtained from, for example, physical modeling [4,5], which is not always possible and/or not always accurate. Also, [4] lists a number of different model assumptions. A different way to obtain a model is from identification [6,7] based on data from the SH wavefront sensor. However, the use of a SH wavefront sensor does not allow for the identification of (dynamic) noncommon path errors. As can be seen in Fig. 1, the optical paths from the incoming wavefront to the wavefront sensor and the path from incoming wavefront to the camera are different. Any additional aberration that occurs in only one of the two paths gives a mismatch between the estimated aberration and the aberration as seen by the camera. This issue is encountered in for example astronomy [8–10] and ophthalmic imaging [11–13].

A phase aberration can be estimated from the camera measurements by using phase retrieval methods [2,3,9,10,14,15]. These techniques use two (or more) images, of which one usually has an added phase diversity. The phase diversity is often a defocus [16,17] since this diversity image can be obtained by simply moving the camera out of focus. From the time series of the estimated phase aberrations, a model can be identified using the same techniques as with the SH wavefront sensor measurements. However, taking multiple images with different phase diversities but the same aberration might be impossible in a dynamical setting, without introducing noncommon paths

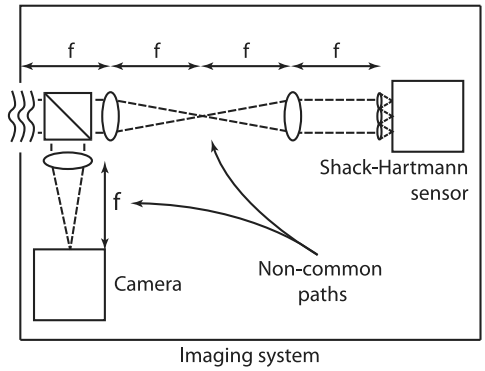

Fig. 1. Classical optical setup for estimating the temporal dynamics of an aberrated wavefront. This setup includes three lenses with focal length f.

in the setup. In addition to the drawback of taking multiple images, the approach to first reconstruct at each time instance the phase aberration and subsequently model the temporal dynamics of the reconstructed aberrations, may suffer from accumulation of the estimation errors in the two-step process. Identification of phase aberration dynamics based on measurements directly with the camera has not yet been investigated. The prior knowledge that the phase aberration behaves in a nonspecific dynamical manner (i.e., the dynamics are contained in a specific model set) has, to our knowledge, not been incorporated previously in a phase aberration estimation procedure.

In this paper, we introduce a method to estimate both phase aberrations and aberration dynamics directly from intensity measurements of the point-spread function (PSF), when the phase aberration dynamics can be described with a vector-valued autoregressive (VAR) model, driven by a stochastic input (see Fig. 2). Here, we circumvent the problem of non-common paths by requiring multiple images for every time step and avoid the accumulation of errors of the two-step process.

To accomplish this, we assume the phase aberrations are small and the PSF can be well approximated by a second-order Taylor series expansion of the image intensities as functions of the Zernike coefficients of the wavefront aberration. We show how the estimation problem has a convex heuristic from which we can iteratively estimate both the phase aberrations and their temporal dynamics.

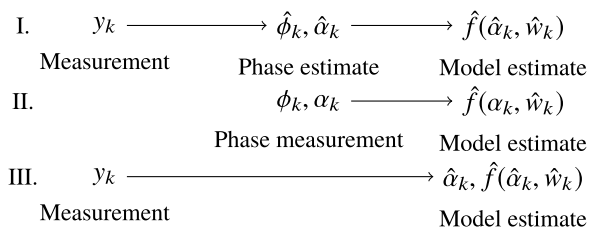

Fig. 2. Overview of identification methods. y denotes the measurement, ϕ is the phase aberration, α is the vector of Zernike coefficients, w_k a noise signal, k is a time index, and $f(\cdot)$ is the model function. I. Phase retrieval first, then model estimation. II. Model estimate based on phase measurements. III. Our method: model estimation and phase retrieval from PSF measurements.

Since we estimate both the aberrations and the dynamics, one way to view this method is as a system identification method with PSF data. A second way to view this method is as a phase retrieval method with a time-evolution model constraint in the pupil plane. In this sense, it also differs from the method in [18,19] where linear, but known, constraints on the phase aberration are used to reduce the parameter search space; our constraints are bilinear. Available literature applicable specifically to noise-driven linear systems with nonlinear outputs seems to be quite sparse. In [20], an identification method is proposed for blind identification of Wiener systems, but an invertible nonlinearity is assumed. Applicable identification methods for these types of systems are based on Bayesian approaches [21–24] using maximum likelihood and expectation maximization algorithms to jointly estimate the dynamics and the nonlinearity itself. However, since the type of nonlinearity is known, we exploit the fact that our estimation problem has a convex heuristic in the sought-after parameters.

Article overview: In Section 2, we set out the mathematical notation, the optical conventions, and the problem statement. Section 3 contains a reformulation of the estimation problem and introduces its convex heuristic. Furthermore, we propose an iterative algorithm that uses the heuristic to compute an estimated model and phase. In Section 4, we conduct a numerical experiment to compare the performance of our method with those of two straightforward approaches. Section 5 contains the conclusion and some suggestions for future research.

A. Notation

In this paper, we make use of the vectorization function $\mathrm{vec}(\cdot): X \to \overline{x}, X \in \mathbb{R}^{m\times n}, \overline{x} \in \mathbb{R}^{mn}$, i.e., a linear transformation of a matrix X into a column vector $\overline{x}$, stacking the columns of X. This transformation is invertible, and we thus also define $\mathrm{vec}^{-1}(\cdot): \overline{x} \to X$. The nuclear norm of a matrix X is defined as $\|X\|_* = \sum_i \sigma_i(X)$, the sum of the singular values of X. $\|X\|_F$ denotes the Frobenius norm of X. As a performance measure, given a true sequence $\{\alpha_k\}_{k=1}^K$ and an estimated sequence $\{\hat{\alpha}_k\}_{k=1}^K$, we define

$$\mathrm{VAF}(\alpha, \hat{\alpha}) = \max\left(0, \left(1 - \frac{\sum_{k=1}^K \|\alpha_k - \hat{\alpha}_k\|_2^2}{\sum_{k=1}^K \|\alpha_k\|_2^2}\right)\right), \tag{1}$$

where VAF is the abbreviation for variance accounted for. Finally, given matrices $X_1, \ldots, X_n$, we define the matrix direct sum as $\oplus_{n=1,\ldots,N} X_n := \mathrm{blkdiag}(X_1, X_2, \ldots, X_N)$, so, e.g.,

$$\bigoplus_{n=1,2} X_n := \mathrm{blkdiag}(X_1, X_2) = \begin{pmatrix} X_1 & 0 \\ 0 & X_2 \end{pmatrix}. \tag{2}$$

2. PROBLEM DESCRIPTION

A. Linear and Quadratic Approximations of the PSF for Small Phase Aberrations

We follow the description of the optical setup in [25] where a linear quadratic controller is designed using quadratic output measurements based on Taylor series expansions of the PSF. The controller is based on a linear time-invariant model of the disturbance. We consider the same optical problem and Taylor approximation setting, but focus on the model identification.

The PSF of an optical system is the Fourier transform of the generalized pupil function (GPF). The GPF is the complex-valued function

$$P(x,y) = \mathbf{A}(x,y)\exp(j\phi(x,y)), \tag{3}$$

where (x,y) are the Cartesian coordinates in the pupil plane, $\mathbf{A}(x,y)$ is the real-valued aperture apodization function, $\phi(x,y)$ is the real-valued phase function, and $j^2 = -1$. We assume that $\phi(x,y) = \phi_a(x,y) + \phi_d(x,y)$, where $\phi_a(x,y)$ is the phase aberration function and $\phi_d(x,y)$ is the phase diversity function. We assume that $\phi_a(x,y)$ can be well approximated by a weighted sum of Zernike basis functions:

$$\overline{\phi}_a(x,y,\alpha) \coloneqq \sum_{r=1}^{s} Z_r(x,y)\alpha_r, \tag{4}$$

where $Z_r(x,y)$ is the rth basis function and $\alpha_r \in \mathbb{R}$ are the weights. Similarly, but with different weights, $\overline{\phi}_d(x,y,\beta)$ approximates $\phi_d(x,y)$. Hence

$$\overline{\phi}(x,y,\alpha,\beta) = \overline{\phi}_a(x,y,\alpha) + \overline{\phi}_d(x,y,\beta),$$

and it follows from the definition in Eq. (4) that

$$\overline{\phi}(x,y,\alpha,\beta) = \overline{\phi}(x,y,\alpha+\beta,0),$$

because of linearity in the weights. Now, we define a grid of points $\tilde{x}\times\tilde{y}$ where $\tilde{x} = \{x_1,\ldots,x_m\}$ and $\tilde{y} = \{y_1,\ldots,y_m\}$. Over this grid, we define

$$\Phi(\alpha,\beta) = \begin{bmatrix} \overline{\phi}(x_1,y_1,\alpha,\beta) & \ldots & \overline{\phi}(x_m,y_1,\alpha,\beta) \\ \vdots & \ldots & \vdots \\ \overline{\phi}(x_1,y_m,\alpha,\beta) & \ldots & \overline{\phi}(x_m,y_m,\alpha,\beta) \end{bmatrix}, \tag{5}$$

and with this definition, we can express the vectorization of $\Phi(\alpha,\beta)$ as a matrix multiplication

$$\mathrm{vec}(\Phi(\alpha,\beta)) = Z(\alpha+\beta), \tag{6}$$

where $Z \in \mathbb{R}^{m^2\times s}$ for a matrix Z composed of $Z_r(x_k,y_k)$. Similarly, we define

$$\Gamma = \begin{bmatrix} \mathbf{A}(x_1,y_1) & \ldots & \mathbf{A}(x_m,y_1) \\ \vdots & \ldots & \vdots \\ \mathbf{A}(x_1,y_m) & \ldots & \mathbf{A}(x_m,y_m) \end{bmatrix}. \tag{7}$$

The complex field in the imaging plane with incoherent illumination is the Fourier transform of the GPF. Taking intensity measurements with a noise-free camera gives the PSF, the squared amplitude of this field:

$$y(\alpha,\beta) = \mathrm{vec}(|\mathcal{F}\{\Gamma\odot\exp(j\mathrm{vec}^{-1}(Z(\alpha+\beta)))\}|^2), \tag{8}$$

where $y(\alpha,\beta) \in \mathbb{R}_+^{p^2}$ and p^2 is the number of pixels, $\odot$ denotes the Hadamard product, $\exp(\cdot)$ denotes the element-wise exponential function, and $|\cdot|^2$ denotes the square of the absolute value of the elements of the matrix.

A linear approximation of the PSF measurements for the ith pixel is given by a first-order Taylor expansion of a small aberration α about the diversity β [25]:

$$y_i(\alpha,\beta) = D_{0,i}(\beta) + D_{1,i}(\beta)\alpha + \mathcal{O}(\|\alpha\|^2), \tag{9}$$

where $\mathcal{O}(\|\alpha\|^2)$ denotes terms of order 2 and higher. The matrices $D_{0,i}$ and $D_{1,i}$ are given, respectively, by

$$D_{0,i}(\beta) = y_i(\alpha,\beta)|_{\alpha=0} \in \mathbb{R},$$
$$D_{1,i}(\beta) = \left.\frac{\partial y_i(\alpha,\beta)}{\partial\alpha}\right|_{\alpha=0} \in \mathbb{R}^{1\times s}. \tag{10}$$

The first-order approximation has limited approximation power. For larger aberrations, a second-order Taylor expansion can be used [25]:

$$y_i(\alpha,\beta) = D_{0,i}(\beta) + D_{1,i}(\beta)\alpha + \frac{1}{2}\alpha^T D_{2,i}(\beta)\alpha + \mathcal{O}(\|\alpha\|^3), \tag{11}$$

where

$$D_{2,i}(\beta) = \left.\frac{\partial^2 y_i(\alpha,\beta)}{\partial\alpha^T\partial\alpha}\right|_{\alpha=0} \in \mathbb{R}^{s\times s}. \tag{12}$$

Since the quadratic approximation holds for aberrations of larger magnitudes, and an identification method that is designed for this approximation would therefore be valid for a larger number of cases, we continue with the model with a quadratic approximation of the PSF and assume $D_{2,i}$ to be nonzero. We use Zernike polynomials normalized to 1 radian amplitude. To give an indication of the validity of the approximation, consider Zernike modes with OSA/ANSI-index 3 to 9. Drawing Zernike coefficients from a normal distribution, the quadratic approximation of the PSF is a good approximation with

$$\mathrm{VAF}(y_i(\alpha,\beta) - D_{0,i}(\beta), D_{1,i}(\beta)\alpha + \frac{1}{2}\alpha^T D_{2,i}(\beta)\alpha)) > 0.9, \tag{13}$$

where VAF stands for variance accounted for (defined in the notation section), for $\|\alpha\|_2 < 1.0$ to 1.4 with defocus diversity β ranging between 0 and 0.5. The linear approximation is invalid without defocus and only valid up to $\|\alpha\|_2 < 0.3$ for $\beta = 0.5$. This trend also holds for similar values of β. Aberrations of small magnitudes can for example be encountered in AO systems operating in a closed loop. See also [26] for a discussion.

B. VAR Models and the Identification Problem

We assume that the total phase $\Phi(\alpha,\beta)$ is time-dependent. In vectorized form, this becomes

$$\mathrm{vec}(\Phi(\alpha_k,\beta_k)) = Z(\alpha_k+\beta_k), \tag{14}$$

where we use k as the time index. Similarly, the ith pixel at time k is denoted with $y_i(\alpha_k,\beta_k)$.

The assumption on the model structure is that the vector of Zernike coefficients of the phase aberration evolves according to a vector-valued autonomous autoregressive model of order N (VAR(N)):

$$\begin{aligned}\alpha_k &= f(\alpha_{k-1},\ldots,\alpha_{k-N},w_k) \\ &= A_1\alpha_{k-1} + \cdots + A_N\alpha_{k-N} + w_k,\end{aligned} \tag{15}$$

where $A_n \in \mathbb{R}^{s\times s}$ are coefficient matrices and $w_k \in \mathbb{R}^s$ is driving, white noise. This is a common dynamic model, for example, for a turbulent phase [4,5,27,28].

The system that generates the measurements $\{y_i(\alpha_k,\beta_k)\}_{k=1,\ldots,K}^{i=1,\ldots,p^2}$ becomes

$$\begin{aligned}\alpha_k &= f(\alpha_{k-1},\ldots,\alpha_N,w_k)\\ &= A_1\alpha_{k-1}+\cdots+A_N\alpha_{k-N}+w_k,\\ y_i(\alpha_k,\beta_k) &= D_{0,i}(\beta_k)+D_{1,i}(\beta_k)\alpha_k+\alpha_k^T D_{2,i}(\beta_k)\alpha_k+v_{i,k},\end{aligned} \tag{16}$$

where $v_{i,k}$ is a noise signal consisting of measurement noise and the approximation error $\mathcal{O}(\|\alpha\|^3)$ in the Taylor expansion of $\overline{\phi}_a$.

The identification problem to find $\{\alpha_k\}_{k=1}^K$, $\{A_n\}_{n=1}^N$, $\{w_k\}_{k=1}^K$, and $\{v_{i,k}\}_{i=1,\ldots,p^2}^{k=1,\ldots,K}$ in Eq. (16) is cast into a minimization problem

$$\begin{aligned}&\underset{A_k,\alpha_k,w_k,v_{i,k}}{\text{minimize}} \sum_{i=1}^{K}\|w_k\|_2^2+\gamma\sum_{k=1}^{K}\sum_{i=1}^{p^2}\|v_{i,k}\|_2^2\\ &\text{subject to } \alpha_k = f(\alpha_{k-1},\ldots,\alpha_N,w_k),\\ &\qquad y_i(\alpha_k,\beta_k) = D_{0,i}(\beta_k)\\ &\qquad\qquad + D_{1,i}(\beta_k)\alpha_k+\alpha_k^T D_{2,i}(\beta_k)\alpha_k+v_{i,k},\end{aligned} \tag{17}$$

for a trade-off parameter $\gamma\in\mathbb{R}_+$. This formulation can be seen as a generalization of a standard state reconstruction problem (see for example [29]), where the difference lies in the quadratic term in the output and the unknown parameter values of the model.

In the following section, we reformulate the equality constraints, which are both bilinear, into rank constraints. Subsequently, we use a heuristic formulation for the rank constraints and create a convex optimization problem.

3. BLIND IDENTIFICATION FROM QUADRATIC MEASUREMENTS

A. Reformulating Equation (17) into a Rank-Constrained Problem

The time evolution of the Zernike coefficients can be written as a matrix equation in the following manner:

$$\underbrace{\begin{pmatrix}\alpha_K & \ldots & \alpha_{N+1}\end{pmatrix}}_{\mathcal{A}_K} = \underbrace{\begin{pmatrix}A_1 & \ldots & A_N\end{pmatrix}}_{A}\underbrace{\begin{pmatrix}\alpha_{K-1} & \alpha_{K-2} & \ldots & \alpha_N\\ \alpha_{K-2} & \alpha_{K-3} & \ldots & \alpha_{N-1}\\ \vdots & \vdots & \vdots & \vdots\\ \alpha_{K-N} & \ldots & \ldots & \alpha_1\end{pmatrix}}_{\mathcal{H}} + W, \tag{18}$$

where $\mathcal{H}$ is a Hankel matrix and $W=\begin{pmatrix}w_K & \ldots & w_{N+1}\end{pmatrix}$. Now, the measurement equations in Eq. (16) can be rearranged to

$$y_i(\alpha_k,\beta_k)-D_{0,i}(\beta_k)-D_{1,i}(\beta_k)\alpha_k-v_{i,k}=\alpha_k^T D_{2,i}(\beta_k)\alpha_k. \tag{19}$$

Furthermore, let $\hat{W}$ be the estimate of W and

$$\begin{aligned}D_y &= \bigoplus_{i,k} y_i(\alpha_k,\beta_k)-D_{0,i}(\beta_k)-D_{1,i}(\beta_k)\alpha_k,\\ D_\alpha &= \bigoplus_{i,k}\alpha_k,\\ D_2 &= \bigoplus_{i,k} D_{2,i}(\beta_k),\\ \hat{V} &= \bigoplus_{i,k} v_{i,k}.\end{aligned} \tag{20}$$

Now, Eq. (17) can be rewritten compactly as

$$\begin{aligned}&\underset{\alpha,A,\hat{W},\hat{V}}{\text{minimize}} \quad \|\hat{W}\|_F^2+\gamma\|\hat{V}\|_F^2\\ &\text{subject to} \quad \mathcal{A}_K-\hat{W}=A\mathcal{H}\\ &\qquad\qquad D_y-\hat{V}=D_\alpha^T D_2 D_\alpha.\end{aligned} \tag{21}$$

The optimization problem in Eq. (21) is an optimization problem with two bilinear equality constraints. Following [30], we will convert these constraints into equivalent rank constraints using Lemma 1.

Lemma 1 ([30]) *Let the matrix-valued function $L(\cdot)$ be defined as*

$$\begin{aligned}&L(A,P,B,C,\mathbf{X},\mathbf{Y})\\ &\quad=\begin{pmatrix}C+AP\mathbf{Y}+\mathbf{X}PB+\mathbf{X}P\mathbf{Y} & (A+\mathbf{X})P\\ P(B+\mathbf{Y}) & P\end{pmatrix}.\end{aligned} \tag{22}$$

For this matrix, it holds that

$$\text{rank}L(A,P,B,C,\mathbf{X},\mathbf{Y})=\text{rank}P \Leftrightarrow APB=C \tag{23}$$

for any choice of $\mathbf{X},\mathbf{Y}$ and any nonzero P of appropriate size.

Define now the two matrices M_{VAR} and M_{meas}, respectively, as

$$\begin{aligned}M_{\text{VAR}} &:= L(A,I_{Ns},\mathcal{H},\mathcal{A}_K-\hat{W},\mathbf{X}_1,\mathbf{Y}_1),\\ M_{\text{meas}} &:= L(D_\alpha^T,D_2,D_\alpha,D_y-\hat{V},\mathbf{X}_2,\mathbf{Y}_2).\end{aligned} \tag{24}$$

Here I_{Ns} is an identity matrix of size $Ns\times Ns$. Applying Lemma 1 to the two constraints in problem (21) gives us

$$\begin{aligned}\text{rank}M_{\text{VAR}} &= \text{rank}I_{Ns}=Ns,\\ \text{rank}M_{\text{meas}} &= \text{rank}D_2\end{aligned} \tag{25}$$

as equivalent constraints. Problem (21) can now be formulated as

$$\begin{aligned}&\underset{\alpha,A,\hat{W},\hat{V}}{\text{minimize}} \quad \|\hat{W}\|_F^2+\gamma\|\hat{V}\|_F^2\\ &\text{subject to} \quad \text{rank}M_{\text{VAR}}=Ns\\ &\qquad\qquad \text{rank}M_{\text{meas}}=\text{rank}D_2.\end{aligned} \tag{26}$$

B. Convex Heuristic for Equation (26)

Rank-constrained problems (or problems with bilinear matrix equalities) are in general NP-hard (nondeterministic polynomial-time hard) to solve [31]. The proposed solution is to solve a convex heuristic for the problem by adding the sum of the nuclear norms of matrices M_{VAR} and M_{meas} in Eq. (25) to the objective function and verifying their rank afterwards. The fact that the two matrices are affinely parameterized by the decision variables A,α_k,w_k, and $v_{i,k}$, even though problem (17) is not, allows applying the nuclear norm to make the problem convex. The advantage of using the nuclear norm is that standard software like YALMIP [32] or CVX [33] is available to implement the convex optimization problem. Alternatively to employing the nuclear norm, other rank-minimizing heuristics could be applied, like for example the use of the truncated nuclear norm [34].

We introduce a regularization parameter λ to weigh the nuclear norms, following from the two rank constraints in Eq. (26), against each other and a parameter ξ to weigh the original objective function with the low-rank inducing terms, and obtain the convex problem

$$\underset{A,\alpha,\hat{W},\hat{V}}{\text{minimize}} \quad \|\hat{W}\|_F^2 + \gamma\|\hat{V}\|_F^2 + \xi(\lambda\|M_{\text{VAR}}\|_* + \|M_{\text{meas}}\|_*). \tag{27}$$

In this optimization problem, $\hat{W}$ appears in the first and third terms [see Eq. (24)], and $\hat{V}$, likewise, in the second and third terms, and there are three parameters (γ, ξ, λ) to tune.

We found it more efficient to work with the following simplified optimization problem with only one single regularization parameter. Define the two matrices Q_{VAR} and Q_{meas}, respectively, as

$$\begin{aligned} Q_{\text{VAR}} &:= L(A, I_{Ns}, \mathcal{H}, \mathcal{A}_K, \mathbf{X}_1, \mathbf{Y}_1), \\ Q_{\text{meas}} &:= L(D_\alpha^T, D_2, D_\alpha, D_y, \mathbf{X}_2, \mathbf{Y}_2). \end{aligned} \tag{28}$$

The size of Q_{VAR} is $(N+1)s \times K + N(s-1)$ and Q_{meas} is a square with sides $(s+1)Kp^2$. The objective function is simplified to

$$\underset{A,\alpha}{\text{minimize}} \ \lambda\|Q_{\text{VAR}}\|_* + \|Q_{\text{meas}}\|_*. \tag{29}$$

If we assume $K \gg N$ and $p^2 \gg s$, and assume that, in general, semi-definite programming problems scale with $O(n^6)$ [35] for problems with n decision variables, then a conservative upper bound for the computational complexity is $O((Kp^2 s)^6)$. The noise terms $\hat{W}$ and $\hat{V}$ are simply interpreted as the feasibility gap of the bilinear matrix equalities with optimal A^* and α_k^*:

$$\begin{aligned} \hat{W}^* &:= \mathcal{A}_K^* - A^*\mathcal{H}^*, \\ \hat{V}^* &:= D_y - (D_\alpha^*)^T D_2 D_\alpha^*. \end{aligned} \tag{30}$$

We observe that Eq. (29) minimizes the feasibility gap (interpreted as the norms of $\hat{W}$ and $\hat{V}$), and we therefore drop the two terms in Eq. (27) that have become redundant.

Since the problem in Eq. (29) is convex in the parameters A and α_k, it is easy to include several forms of prior information through the use of convex constraints, or regularization of the objective function. Examples are constraints expressing an affine parameter dependence of matrix A, or the inclusion of an additional term to the objective function, such as $\mu\|A\|_F^2$, for some regularization parameter μ, to prevent the elements of matrix A from having large magnitudes.

The optimization in Eq. (29) can be performed for different choices of the parameters $\mathbf{X}_1, \mathbf{Y}_1, \mathbf{X}_2$, and $\mathbf{Y}_2$. This freedom can be used in an iterative manner, as outlined in Algorithm 1.

Algorithm 1. Sequential convex optimization-based identification

1: **procedure** SCOBI
2: **while** not converged **do**
3: Solve Eq. (29) with parameters $\mathbf{X}_1, \mathbf{Y}_1, \mathbf{X}_2, \mathbf{Y}_2$ to obtain optimal $A^*, \mathcal{A}_K^*, D_\alpha^*$, and D_y^*.
4: Set

$$\begin{aligned} \mathbf{X}_1^+ &= -A^*, \qquad \mathbf{Y}_1^+ = -\mathcal{A}_K^*, \\ \mathbf{X}_2^+ &= -(D_\alpha^*)^T, \qquad \mathbf{Y}_2^+ = -D_\alpha^*. \end{aligned} \tag{31}$$

5: **end while**
6: **end procedure**

4. NUMERICAL EXPERIMENTS

A. Experimental Setting

To test the performance of Algorithm 1, we generate data for two separate identification experiments as described below.

We assume that the time-varying aberration consists of oblique astigmatism and coma and the diversity of only a defocus. That is, we consider a case with $s = 3$ aberrated Zernike modes, so

$$\overline{\phi}(\alpha_k, \beta_k) = Z_2^{-2}\alpha_k(1) + Z_3^{-1}\alpha_k(2) + Z_3^1\alpha_k(3) + Z_2^0\beta_k. \tag{32}$$

The first mode, Z_2^{-2}, is an even mode and the effect is that without an added diversity, $\alpha(1)$ and $-\alpha(1)$ are indistinguishable from a single PSF measurement.

In the first experiment, every tenth measurement is taken with a defocus diversity and the remaining 90% of the images are taken without diversity ($\beta_k = 0$). That is,

$$\beta_k = \begin{cases} 0.5 & k = 1, 11, 21, \ldots \\ 0 & \text{otherwise} \end{cases} \qquad \text{(Experiment 1)}. \tag{33}$$

The motivation is that the out-of-focus images are used to distinguish between $\alpha_k(1)$ and $-\alpha_k(1)$, and the use of the model-set constraint determines the sign for the remaining in-focus images.

In the second experiment, every image is taken out of focus, i.e.,

$$\beta_k = 0.5 \ \forall \ k \quad \text{(Experiment 2)}. \tag{34}$$

For both experiments, the coefficients α evolve according to a VAR(2) model. The state-space formulation of the VAR model has the system matrix

$$A_s = \begin{pmatrix} A_1^{\text{true}} & A_2^{\text{true}} \\ I & 0 \end{pmatrix}, \tag{35}$$

where the block matrix $(A_1^{\text{true}} \quad A_2^{\text{true}})$ is random and the poles of A_s have absolute value between 0.75 and 0.9. Thus, the poles are chosen to be relatively "slow" (toward the edge of the unit circle). The effect of this choice is that their corresponding dynamics are more clearly present in a relatively short data set. The decorrelation time of the states of a representative randomly generated system is approximately 40–50 samples. These two experiments are repeated 100 times with different system matrices A_s, state, and measurement noise sequences for every repetition. Parameter settings are listed in Table 1. In both experiments, the driving noise w has a noise power that ensures that $\mathcal{O}(\|\alpha\|^3)$ is small. Both the driving noise and measurement noise are Gaussian white noise with mean and variance as specified in Table 1. From the PSF generated according to Eq. (8), we use a subset of (only) 25 pixels (see Fig. 3). The number of pixels that are used is limited to reduce the computation time of the optimization, which is roughly 800 s on a desktop computer. The initial guess for $\mathbf{X}_1, \mathbf{X}_2, \mathbf{Y}_1, \mathbf{Y}_2$ is drawn

Table 1. Settings for the Two Numerical Experiments

	Experiment 1	Experiment 2
w_k	$N(0, 3 \cdot 10^{-2} I)$	$N(0, 2 \cdot 10^{-1} I)$
Measurement noise in v_k	$N(0, 1 \cdot 10^{-7} I)$	$N(0, 1 \cdot 10^{-5} I)$
Time series K	100	100
VAR order N	2	2
Pixels p^2	25	25
Iterations Alg. 1	150	150
Repetitions	100	100

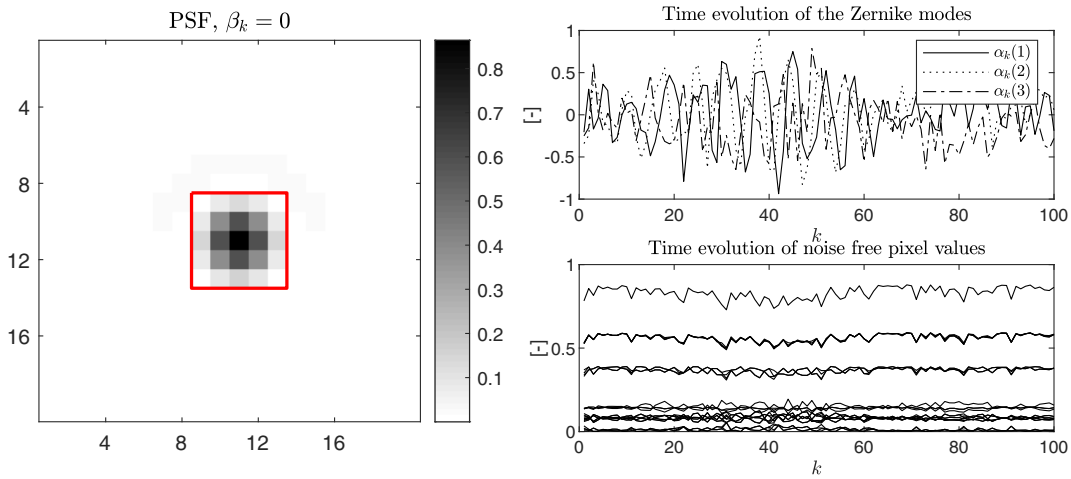

Fig. 3. On the left is the PSF at a time step of $k = 100$. Outlined in red are the 25 pixel values used in the identification. On the right, top, are the Zernike coefficients for an example data set for $k = 1, \ldots, 100$. At the bottom are the time series for $k = 1, \ldots, 100$ for the corresponding pixel values.

randomly from a normal distribution $N(0, 10^{-5}I)$. The problem in Eq. (29) is solved for $\lambda = 0.25, 0.5, \ldots, 0.25 \cdot (z-1), 0.25 \cdot z$, where $\lambda = 0.25 \cdot z$ corresponds to the first solution that worsens the VAF of the states compared with the corresponding solution for $\lambda = 0.25 \cdot (z-1)$. A small regularization of the form $0.005\|A\|_F^2$ is added to avoid over-fitting of the model to the estimated state sequence. A side effect is that it reduces the spectral radius [36].

B. Alternative Methods

For benchmarking purposes, we consider two alternative methods to our proposed method for solving Eq. (17).

Two-step least squares: The first alternative is to estimate the system dynamics in a two-step method based on the linear approximation. It has the following two steps:

$$\text{I)}\ \hat{\alpha} = \arg\min_{\alpha} \sum_{i,k} \|y_i(\alpha_k, \beta_k) - D_{0,i}(\beta_k) - D_{1,i}(\beta_k)\alpha_k\|_F^2,$$
$$\text{II)}\ (\hat{A}_1, \hat{A}_2) = \arg\min_{A_1, A_2} \sum_{k} \|\hat{\alpha}_k - A_1\hat{\alpha}_{k-1} - A_2\hat{\alpha}_{k-2}\|_F^2. \quad (36)$$

For images taken without diversity, the first problem is ill-conditioned, and this method is not applicable.

Separable nonlinear least squares (SNLLSs): The second method minimizes a nonlinear least squares cost function that exploits the separability of the optimization problem. For the minimization, we use MATLAB's built-in nonlinear least squares optimizer where we can make use of an exact or approximate gradient (for settings, see Appendix B). That is, the identification problem can also be formulated as

$$\underset{A,\alpha}{\text{minimize}}\ \|G(\alpha)\bar{A} + h(\alpha)\|_2^2; \quad (37)$$

$\bar{A} = \text{vec}(A)$, and G and h are given in Appendix A.

The first step is to optimize over $\bar{A}$ and then substitute the optimal solution $\bar{A}(\alpha) = -G^{\dagger}(\alpha)h(\alpha)$ into Eq. (37), which yields the problem

$$\begin{aligned} &\underset{A,\alpha}{\text{minimize}}\ \|G\bar{A} + h\|_2^2 \\ &= \underset{\alpha}{\text{minimize}}\ \|(I - GG^{\dagger})h\|_2^2 \\ &= \underset{\alpha}{\text{minimize}}\ \|P_G^{\perp}h\|_2^2, \end{aligned} \quad (38)$$

which may be solved using a nonlinear least squares solver. With the residual, $r = G\bar{A}(\alpha) + h = P_G^{\perp}h$, the solver can be fed either the exact gradient

$$\frac{\partial r}{\partial \alpha} = \frac{\partial P_G^{\perp}}{\partial \alpha}h + P_G^{\perp}\frac{\partial h}{\partial \alpha} \quad (39)$$

or an approximate gradient

$$\frac{\partial r}{\partial \alpha} \approx P_G^{\perp}\left(\frac{\partial G}{\partial \alpha} + \frac{\partial h}{\partial \alpha}\right), \quad (40)$$

which is considerably faster computationally [37]. The solver was initialized in three different ways: first, with the results from the two-step least squares; second, with the result of our proposed method; and third, with 100 random initial guesses. This number corresponds to solving the same problem with the proposed method in terms of computational time.

C. Performance Measures

We compare the estimation results in two ways. First, we compare the estimated state sequence (Zernike coefficients). Second, we compare how well the estimated dynamics can be used to predict a state of an independent data set generated under the same circumstances as the data set used for identification. The estimation error for an estimated $\hat{A}_1$ and $\hat{A}_2$ is defined as

$$e_k = \alpha_k - \hat{A}_1\alpha_{k-1} - \hat{A}_2\alpha_{k-2}. \quad (41)$$

D. Results and Discussion

Despite the benefit of several random initial guesses for each experiment, the SNLLS method consistently failed to produce good results for any of the experiments. Thus, the results of random initial guesses are omitted from the results. In the

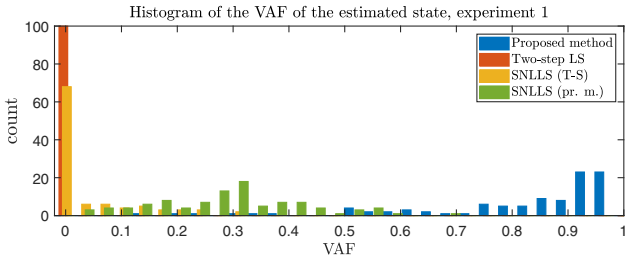

Fig. 4. VAF of the estimated state sequences for the first experiment. T-S is for the initial guess from the two-step least squares and pr.m. is for the initial guess from the solution of the proposed method. Note that from this figure, it is apparent that the first least squares problem of the two-step least squares solution (36) fails to produce a good estimate of the states.

experiments, it was noted that initialization with the correct solution in the SNLLS algorithm yields the correct solution. However, with small perturbations of this initialization, the solution will instead converge to a different local minimum with the SNLLS method. We conclude that the SNLLS method is very sensitive to the initialization. The VAF of the estimated states are displayed in the histogram in Figs. 4 and 5. We draw two conclusions from these figures.

First, the proposed method is the only one that can correctly identify the states in Experiment 1 (top histogram). In most instances, the estimated states were close to the true states, even though 90% of the images were taken without added phase diversity.

Second, the proposed method, with its quadratic approximation of the measurements, outperforms the linear model of the measurements (bottom histogram) in Experiment 2.

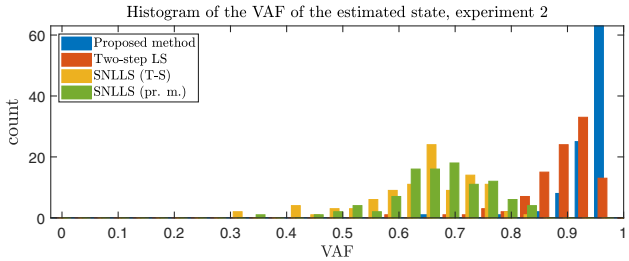

Fig. 5. VAF of the estimated state sequences for the second experiment. T-S is for the initial guess from the two-step least squares and pr.m. is for the initial guess from the solution of the proposed method.

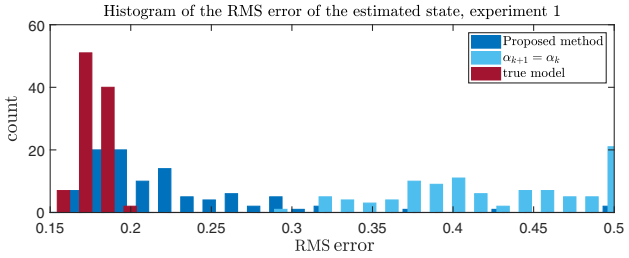

Fig. 6. Comparison of RMS error for the next predicted state by the proposed method, states remain constant, and the true model for the first experiment.

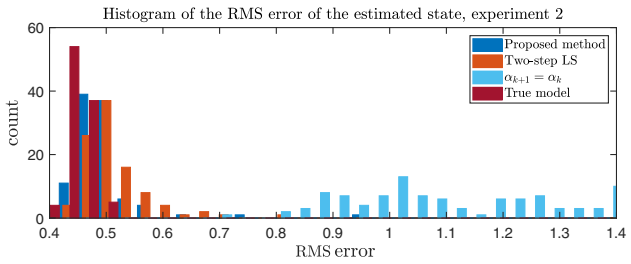

Fig. 7. Comparison of RMS for the next predicted state by the proposed method, states remain constant, and the true model for the first experiment.

In Figs. 6 and 7, we compare the average root mean square (RMS) error of the state estimates for the validation data sets. The SNLLS method produced bad estimates in terms of RMS error, on average about 1000 times worse compared with the proposed method. Thus, it is left out of these figures. We give the RMS estimation error produced by the true model, and the average RMS estimation error produced by the static model $\alpha_{k+1} = \alpha_k$ for comparison. From these figures, we conclude that the proposed method can identify the true model with good performance, since its performance is close to that of the true model, and that it significantly improves upon the assumption of a static aberration.

Some of the limitations we found that worsened the estimation results, were increasing noise levels, and the limitations of the quadratic approximation when the aberration increased in strength. Also, with the relatively short data set we used, it was more difficult to estimate fast dynamics.

5. CONCLUSION AND FUTURE RESEARCH

We presented a method to jointly estimate the temporal dynamics of a phase aberration and the phase aberration itself of an optical system based on measurements of the PSF of the optical system. The approach is novel first in the sense that a model set of temporal dynamics is used as prior information for phase retrieval, and second, as it uses a convex heuristic approach with good results to a blind system identification problem with a nonlinear output function. Future research lines include modeling spatial dynamics in anisoplanatism instead of temporal dynamics and increasing the accuracy of the (small) phase approximation for larger phase aberrations.

APPENDIX A: MATRICES IN EQ. (37)

$$G = \begin{pmatrix} I_n \otimes \alpha_{K-1}^T & I_n \otimes \alpha_{K-2}^T & \dots & I_n \otimes \alpha_{K-M}^T \\ \vdots & \vdots & \vdots & \vdots \\ I_n \otimes \alpha_{K-N}^T & \dots & \dots & I_n \otimes \alpha_1^T \\ 0 & 0 & & \\ \vdots & \vdots & \vdots & \vdots \\ 0 & 0 & & \end{pmatrix}, \tag{A1}$$

$$h = \begin{pmatrix} -\alpha_K \\ \vdots \\ -\alpha_{N+1} \\ y_{1,K} - D_{0,1}(\beta_k) - D_{1,1}(\beta_k)\alpha_K - \alpha_K^T D_{2,1}(\beta_k)\alpha_K \\ \vdots \\ y_{p^2,K} - D_{0,p^2}(\beta_k) - D_{1,p^2}(\beta_k)\alpha_K - \alpha_K^T D_{2,p^2}(\beta_k)\alpha_K \\ \vdots \\ y_{1,1} - D_{0,1}(\beta_k) - D_{1,1}(\beta_k)\alpha_K - \alpha_K^T D_{2,1}(\beta_k)\alpha_K \\ \vdots \\ y_{p^2,1} - D_{0,p^2}(\beta_k) - D_{1,p^2}(\beta_k)\alpha_1 - \alpha_1^T D_{2,p^2}(\beta_k)\alpha_1 \end{pmatrix}. \tag{A2}$$

APPENDIX B: SETTINGS OF THE NONLINEAR SOLVER

Apart from `SpecifyObjectiveGradient=true`, default settings for `lsqnonlin` have been used for all experiments involving SNLLSs. For a complete list of the default settings, we refer to MATLAB's official documentation.

Funding. Seventh Framework Programme (FP7) (339681); Vetenskapsrådet (VR) (E05946CI).

REFERENCES

1. B. C. Platt and R. Shack, "History and principles of Shack–Hartmann wavefront sensing," J. Refractive Surg. **17**, S573–S577 (2001).
2. D. Acton, D. Soltau, and W. Schmidt, "Full-field wavefront measurements with phase diversity," Astron. Astrophys. **309**, 661–672 (1996).
3. L. Mugnier, J.-F. Sauvage, T. Fusco, A. Cornia, and S. Dandy, "On-line long-exposure phase diversity: a powerful tool for sensing quasi-static aberrations of extreme adaptive optics imaging systems," Opt. Express **16**, 18406–18416 (2008).
4. C. Kulcsár, H.-F. Raynaud, J.-M. Conan, C. Correia, and C. Petit, "Control design and turbulent phase models in adaptive optics: a state-space interpretation," in *Adaptive Optics: Methods, Analysis and Applications* (Optical Society of America, 2009), paper AOWB1.
5. B. Le Roux, J.-M. Conan, C. Kulcsár, H.-F. Raynaud, L. M. Mugnier, and T. Fusco, "Optimal control law for classical and multiconjugate adaptive optics," J. Opt. Soc. Am. A **21**, 1261–1276 (2004).
6. K. Hinnen, M. Verhaegen, and N. Doelman, "A data-driven H2-optimal control approach for adaptive optics," IEEE Trans. Control Syst. Technol. **16**, 381–395 (2008).
7. M. Verhaegen and V. Verdult, *Filtering and System Identification: a Least Squares Approach* (Cambridge University, 2007).
8. M. Hartung, A. Blanc, T. Fusco, F. Lacombe, L. Mugnier, G. Rousset, and R. Lenzen, "Calibration of NAOS and CONICA static aberrations—experimental results," Astron. Astrophys. **399**, 385–394 (2003).
9. A. Blanc, T. Fusco, M. Hartung, L. Mugnier, and G. Rousset, "Calibration of NAOS and CONICA static aberrations—application of the phase diversity technique," Astron. Astrophys. **399**, 373–383 (2003).
10. M. A. van Dam, D. Le Mignant, and B. A. Macintosh, "Performance of the Keck observatory adaptive-optics system," Appl. Opt. **43**, 5458–5467 (2004).
11. A. Roorda, F. Romero-Borja, and W. J. Donnelly III, H. Queener, T. J. Hebert, and M. C. Campbell, "Adaptive optics scanning laser ophthalmoscopy," Opt. Express **10**, 405–412 (2002).
12. H. Hofer, N. Sredar, H. Queener, C. Li, and J. Porter, "Wavefront sensorless adaptive optics ophthalmoscopy in the human eye," Opt. Express **19**, 14160–14171 (2011).
13. Y. N. Sulai and A. Dubra, "Non-common path aberration correction in an adaptive optics scanning ophthalmoscope," Biomed. Opt. Express **5**, 3059–3073 (2014).
14. T. Fusco, C. Petit, G. Rousset, J. F. Sauvage, A. Blanc, J. M. Conan, and J. L. Beuzit, "Optimization of the pre-compensation of non-common path aberrations for adaptive optics systems," in *Adaptive Optics: Methods, Analysis and Applications* (Optical Society of America, 2005), paper AWB2.
15. J.-F. Sauvage, T. Fusco, G. Rousset, and C. Petit, "Calibration and precompensation of noncommon path aberrations for extreme adaptive optics," J. Opt. Soc. Am. A **24**, 2334–2346 (2007).
16. R. A. Gonsalves, "Phase retrieval and diversity in adaptive optics," Opt. Eng. **21**, 215829 (1982).
17. J. R. Fienup, "Phase retrieval algorithms: a comparison," Appl. Opt. **21**, 2758–2769 (1982).
18. M. G. Lofdahl, "Multi-frame blind deconvolution with linear equality constraints," in *Image Reconstruction from Incomplete Data II* (International Society for Optics and Photonics, 2002), Vol. **4792**, pp. 146–156.
19. M. Van Noort, L. R. Van Der Voort, and M. G. Löfdahl, "Solar image restoration by use of multi-frame blind de-convolution with multiple objects and phase diversity," Solar Phys. **228**, 191–215 (2005).
20. L. Vanbeylen, R. Pintelon, and J. Schoukens, "Blind maximum-likelihood identification of Wiener systems," IEEE Trans. Signal Process. **57**, 3017–3029 (2009).
21. A. Wills, T. B. Schön, L. Ljung, and B. Ninness, "Blind identification of Wiener models," in *Proceedings of the 18th IFAC World Congress*, Milan, Italy (2011).
22. A. Wills, T. B. Schön, L. Ljung, and B. Ninness, "Identification of Hammerstein–Wiener models," Automatica **49**, 70–81 (2013).
23. F. Lindsten, T. B. Schön, and M. I. Jordan, "Bayesian semiparametric Wiener system identification," Automatica **49**, 2053–2063 (2013).
24. F. Lindsten, T. Schön, and M. I. Jordan, *A Semiparametric Bayesian Approach to Wiener System Identification* (Linköping University Electronic, 2011).
25. R. Marinică, C. S. Smith, and M. Verhaegen, "State feedback control with quadratic output for wavefront correction in adaptive optics," in *IEEE 52nd Annual Conference on Decision and Control (CDC)* (IEEE, 2013), pp. 3475–3480.
26. C. Smith, R. Marinică, A. Den Dekker, M. Verhaegen, V. Korkiakoski, C. Keller, and N. Doelman, "Iterative linear focal-plane wavefront correction," J. Opt. Soc. Am. A **30**, 2002–2011 (2013).
27. G. Monchen, B. Sinquin, and M. Verhaegen, "Recursive Kronecker-based vector autoregressive identification for large-scale adaptive optics," IEEE Trans. Control Syst. Technol. **99**, 1–8 (2018).
28. B. Sinquin and M. Verhaegen, "Quarks: identification of large-scale Kronecker vector-autoregressive models," IEEE Trans. Autom. Control **64**, 448–463 (2019).
29. N. Haverbeke, "Efficient numerical methods for moving horizon," dissertation (Katholieke Universiteit Leuven, 2011).
30. R. Doelman and M. Verhaegen, "Sequential convex relaxation for convex optimization with bilinear matrix equalities," in *Proceedings of the European Control Conference* (2016).
31. O. Toker and H. Ozbay, "On the NP-hardness of solving bilinear matrix inequalities and simultaneous stabilization with static output feedback," in *Proceedings of the American Control Conference* (IEEE, 1995), Vol. **4**, pp. 2525–2526.
32. J. Lofberg, "YALMIP: a toolbox for modeling and optimization in MATLAB," in *IEEE International Symposium on Computer Aided Control Systems Design* (IEEE, 2004), pp. 284–289.
33. M. Grant and S. Boyd, "CVX: MATLAB software for disciplined convex programming, version 2.1," 2014, http://cvxr.com/cvx.

34. Y. Hu, D. Zhang, J. Ye, X. Li, and X. He, "Fast and accurate matrix completion via truncated nuclear norm regularization," IEEE Trans. Pattern Anal. Mach. Intell. **35**, 2117–2130 (2013).
35. L. Vandenberghe, V. R. Balakrishnan, R. Wallin, A. Hansson, and T. Roh, "Interior-point algorithms for semidefinite programming problems derived from the KYP lemma," in *Positive Polynomials in Control* (Springer, 2005), pp. 195–238.
36. T. Van Gestel, J. A. Suykens, P. Van Dooren, and B. De Moor, "Identification of stable models in subspace identification by using regularization," IEEE Trans. Autom. Control **46**, 1416–1420 (2001).
37. R. Wallin and A. Hansson, "Maximum likelihood estimation of linear SISO models subject to missing output data and missing input data," Int. J. Control **87**, 2358–2364 (2014).